

Overexpression of Long Noncoding RNA *HOTAIR* Is a Unique Epigenetic Characteristic of Myxopapillary Ependymoma

Haiyin Zheng, MBBS, PhD, Katherina Baranova, MD, Jun Song, MBBS, PhD, Lei Yan, MD, PhD, Saumik Biswas, PhD, Subrata Chakrabarti, MBBS, PhD, and Qi Zhang , MBBS, PhD

Abstract

Ependymomas are a heterogeneous group of central nervous system tumors. Despite the recent advances, there are no specific biomarkers for ependymomas. In this study, we explored the role of homeobox (*HOX*) genes and long noncoding RNA (lncRNA) *HOTAIR* in ependymomas along the neural axis. Bioinformatics analysis was performed on publicly available gene expression data. Quantitative RT-PCR was used to determine the mRNA expression level among different groups of ependymomas. RNA in situ hybridization (ISH) with probes specific to *HOTAIR* was performed on tumor tissue microarray (TMA) constructed with 19 ependymomas formalin-fixed paraffin-embedded tissue. Gene expression analysis revealed higher expression of posterior *HOX* genes and *HOTAIR* in myxopapillary ependymoma (MPE), in comparison to other spinal and intracranial ependymoma. qRT-PCR confirmed the high *HOXD10* expression in spinal MPEs. There was a significant upregulation of *HOTAIR* expression in spinal MPE and elevated *HOTAIR* expressions were further confirmed by RNA ISH on the TMA. Intriguingly, *HOXD10* and *HOTAIR* expressions were not elevated in nonpendymoma spinal tumors. Our collective results suggest an important role for the lncRNA *HOTAIR* and posterior *HOX* genes in the tumorigenesis of spinal MPE. *HOTAIR* may also serve as a potential diagnostic marker for spinal MPE.

Key Words: *HOTAIR*, *HOX*, lncRNA, Myxopapillary ependymoma, Spinal tumors.

From the Department of Pathology and Laboratory Medicine, Western University (HZ, KB, JS, LY, SB, SC, QZ); Department of Pathology and Laboratory Medicine, London Health Sciences Centre (SC, QZ), London, Ontario, Canada; College of Integrative Medicine, Fujian University of Traditional Chinese Medicine (HZ); and Department of Cell Biology and Genetics, School of Basic Medical Sciences, Fujian Medical University (JS), Fuzhou, Fujian, PR China.

Send correspondence to: Qi Zhang, MBBS, PhD, Department of Pathology and Laboratory Medicine, London Health Sciences Centre, Western University, 339 Windermere Road, London, ON, Canada N6A 5A5; E-mail: qzhan33@uwo.ca

This study was in part supported by the Western University Pathology Internal Funds for Academic Development and the Brain Tumor Foundation of Canada Research Grant (QZ). (QZ).

The authors have no duality or conflicts of interest to declare.

Supplementary Data can be found at academic.oup.com/jnen.

INTRODUCTION

Ependymomas are a heterogeneous group of central nervous system (CNS) tumors occurring along the entire neural axis. The 2016 World Health Organization (WHO) classification of CNS tumors recognizes 9 subgroups of ependymomas based on the anatomic location and molecular signature (1). Myxopapillary ependymomas (MPE) represent ~10% of all ependymomas, with unique localization and morphology. MPE arises almost exclusively in lumbosacral region (conus medullaris, cauda equina, and filum terminale). The typical MPE is classified as WHO grade I; however, tumor recurrence and more aggressive clinical behavior are observed in the pediatric population and patients with incomplete surgical resection. In fact, the Consortium to Inform Molecular and Practical Approaches to CNS Tumor Taxonomy (cIMPACT-NOW) working group recommended designating MPE as WHO grade II in their most recent update 7 (2). Despite the extensive genetic and epigenetic analysis of ependymomas, little is known about the molecular characteristics of MPEs (3, 4). With gene expression microarray analysis, Barton et al identified a distinct expression profile in 5 pediatric MPEs in comparison to intracranial ependymomas (IC-EPNs) (5). Among the top 15 overexpressed genes in MPEs, 6 are posterior Homeobox (*HOX*) genes. The overexpression of selected *HOX* genes (*HOXB13* and *HOXA9*) in MPE was confirmed with immunohistochemistry (5, 6).

HOX genes are a family of transcription factors characterized by possessing a highly conserved homeodomain, which was originally discovered in *Drosophila*. *HOX* genes play important roles in the anterior-posterior (A-P) body axis patterning and nervous system development in all animal species (6, 7). In most vertebrates, there are at least 39 *HOX* genes organized in 4 clusters: *HOXA*, *HOXB*, *HOXC*, and *HOXD*. Each *HOX* gene cluster contains a subset of 13 paralogous groups (*HOX1-13*). In humans, the 4 *HOX* clusters (*HOX A-D*) are localized on 4 chromosomes (chromosomes 7, 17, 12, and 2, respectively). The *HOX* genes are positioned in a 3' to 5' fashion corresponding to their expression along the A-P axis in animals (spatial collinearity). Deregulation of *HOX* expression pattern is identified in abnormal development and recently in tumorigenesis (8).

The *HOX* gene expression is regulated by long non-coding RNAs (lncRNA). LncRNAs can either activate or repress their target *HOX* gene expression. Recently, the lncRNA *HOX* Antisense Intergenic RNA (*HOTAIR*) has been shown to play an important role in *HOX* gene regulation (9). As the name indicates, *HOTAIR* is transcribed in an antisense direction by RNA polymerase II and arises from the intergenic region between *HOXC11* and *HOXC12* within the *HOXC* cluster. Studies have shown that *HOTAIR* induces transcriptional silencing of the *HOXD* locus on chromosome 2 by recruiting the polycomb repressive complex 2 (*PRC2*), which trimethylates lysine 27 of histone H3 (H3K27me3), and in turn executes epigenetic silencing during embryonic development (10). In addition, *HOTAIR* is involved in multiple processes associated with oncogenesis, such as cell proliferation, apoptosis, invasion, aggression, and metastasis (10, 11, 12). On the basis of these functions, *HOTAIR* is considered a potential biomarker for cancers of various systems, including breast (13), lung (14), liver (15), gastrointestinal tract (16, 17), and CNS (glioblastoma) (18).

In light of the *HOX* gene patterning function in human A-P axis (the unique sacrolumbar location of MPE) and the overexpression of selected posterior *HOX* genes in pediatric MPEs, we explored the role of *HOX* genes in ependymomas along the neural axis, with a focus on MPEs. We also investigated the role of the lncRNA *HOTAIR* in ependymomas and nonependymoma spinal tumors.

MATERIALS AND METHODS

Study Cohort

Two datasets of gene expression microarray data were used for bioinformatics analysis. The first dataset was retrieved from the Gene Expression Omnibus (GEO) at accession GSE64415 (4, 19, 20). This dataset constituted Affymetrix HG U133 Plus 2.0 microarray Robust Multichip Average (RMA) normalized gene expression data from 209 ependymal tumor samples (8 MPE, 11 spinal, and 198 IC-EPN). The second dataset was retrieved from GEO at accession GSE66787 (21). This dataset consisted of Affymetrix Human Gene 1.1 ST Array expression data for 35 spinal ependymomas (20 MPE, 15 spinal ependymomas). The second microarray dataset did not contain probes for *HOTAIR* but did include data for the *HOX* genes of interest.

A retrospective case search was performed from the Department of Pathology and Laboratory Medicine at London Health Sciences Centre (LHSC), with approval by the research ethics board of Western University (HSREB 111911). Nineteen formalin-fixed paraffin-embedded (FFPE) ependymoma samples (5 MPE, 7 spinal, and 7 IC-EPNs) were obtained from LHSC for tissue microarray construction, immunohistochemistry and RNA in situ hybridization (ISH). Forty-one snap-frozen tumor samples (8 MPE, 3 spinal, and 20 IC-EPN, 10 nonependymoma spinal tumors) were obtained from the Brain Tumor Tissue Bank of Canada and the Hospital for Sick Children Tumor Bank for qRT-PCR analysis. The group of nonependymoma spinal tumors is composed of 5 schwannoma, 3 neuroblastoma/ganglioneuroma, 1 pilocytic astrocy-

toma, and 1 osteochondroma. All cases were histologically reviewed by a neuropathologist (QZ). No patient received neoadjuvant treatment prior to the surgical removal of the tumor.

Bioinformatics

A full list of *HOX* genes were pulled from the literature (20). The list of genes was converted to the corresponding microarray probe identifier using Ensembl's BioMart application (22, 23). The microarray datasets were downloaded and the probe sets corresponding to our genes of interest were extracted from the overall dataset. The probe with the highest average expression was used when multiple probes for the same genes existed. Gene expression analysis for the microarray datasets was completed in R (24). Gene expression and sample data were hierarchically clustered by row and column and a heatmap was produced using the R package "ggplot2" (25). For heatmap analysis, the microarray data were scaled to have a mean of 0 and a standard deviation of 1. Data above a normalized value of 2 were set to 2, and data below -2 were set to -2 for over and underexpression, respectively. Violin plots with overlaid box plots were produced on gene expression data for the 209 ependymomas between spine, posterior fossa, and supratentorial ependymomas using R ggplot2 with the extension package "ggstatsplot" for statistical analysis (26).

RNA Extraction and qRT-PCR Analysis

Total RNA was extracted from the frozen tumor tissue using RNeasy Plus Mini Kit (QIAGEN, Toronto, Canada). For qRT-PCR, 1 µg of total RNA was reverse transcribed to cDNA using RT2 First Strand Kit (QIAGEN). Real-time PCR analysis was performed with TB Green Advantage qPCR Premix (Takara Bio, Mountain View, CA). The primers were listed in [Supplementary Data Table S1](#). qRT-PCR and data collection were performed using the LightCycler 96 instrument (Roche Diagnostics Canada, Laval, Quebec, Canada). LightCycler 96 SW 1.1 software (Roche) was used for data analysis and relative RNA expression levels were calculated by standard curve method using β -actin as an internal control for sample normalization.

Tumor Tissue Microarray Construction

Representative tumor FFPE blocks were selected based on the hematoxylin and eosin (H&E) sections. Three 1-mm cores from the region of interests in each tumor block were sampled and inserted in a recipient paraffin block, using a semi-automatic tissue arrayer (Galileo CK 2500, Integrated Systems Engineering, Milan, Italy). This allowed a triplicate sampling of 19 tumors in 1 tumor tissue microarray (TMA) block.

Immunohistochemistry

The paraffin-embedded tissue and TMA blocks were sectioned into 4 µm tissue slices with a microtome and placed on supercharged glass slides. Immunohistochemistry (IHC) was performed using Dako Autostainer Link 48 according to

TABLE. Patient Demographic Information

	*GEO 1 (GSE64415)			*GEO 2 (GSE66787)			LHSC		
	MPE	SP-EPN	IC-EPN	MPE	SP-EPN	IC-EPN	MPE	SP-EPN	IC-EPN
n =	8	11	198	20	15	0	15	8	27
Age (years)									
Range	9–58	5–55	0.75–70	7–55	14–68		7–59	28–71	1–62
Mean	31	33	17	30	39		27	44	27
Sex									
Male	6 (75%)	6 (55%)	99 (52%)	6 (33%)	8 (57%)		12 (80%)	4 (50%)	11 (41%)
Female	2 (25%)	5 (45%)	91 (48%)	12 (67%)	6 (43%)		3 (20%)	4 (50%)	16 (59%)

The data “age” is unavailable for 34 cases in the GEO1 cohort and 1 case in GEO2 cohort. The data “sex” is unavailable for 3 cases in the GEO2 cohort.

the user’s manual (Dako, Santa Clara, CA). Primary antibodies include glial fibrillary acidic protein (GFAP, 1:20 000, rabbit polyclonal; Dako), Cytokeratin AE1/AE3 (CK AE1/AE3, mouse monoclonal; Dako GA053), epithelial membrane antigen (EMA, mouse monoclonal; Dako IR629), trimethylated Histone H3 at lysine 27 (H3K27me3, 1:500, Rabbit polyclonal; Millipore 07-449).

RNA ISH

RNA ISH was performed with a human *HOTAIR* probe (RNAscope LS 2.5 Probe-Hs-*HOTAIR*, 312348, Advanced Cell Diagnostics, Newark, CA), on the Leica Biosystems BOND RX platform according to the user’s manual. In brief, the TMA sections were baked and deparaffinized, followed by target retrieval (15 minutes at 95°C using Leica Epitope Retrieval Buffer 2) and protease treatment (15 minutes at 40°C). Probes were then hybridized for 2 hours at 42°C followed by RNAscope amplification. DAB chromogenic detection was then performed.

Image Analysis

The glass slides (H&E, IHC, and RNA ISH) were scanned at 40× magnification using automated scanning system (Aperio XT, Leica Biosystems). The digitalized slides were analyzed with QuPath software according to the user’s instruction and scientific publications (27, 28). In brief, the “TMA dearrayer” command was used to identify each tissue core, followed by the “tissue detection” command to identify total tissue area. Detected tissue was then manually edited to remove areas of nonspecific staining and to identify areas of interest. Positive pixel count was used in the areas of interest using the “positive pixel count” command for DAB chromogenic optical intensity of *HOTAIR* hybridization. “Negative pixel” is based on the nuclear hematoxylin counterstain. A score of positive pixel index (PI, positive pixel %) was calculated as: Positive pixel % = (positive pixel count)/(positive pixel count + negative pixel count) * 100. PI was used for statistical analysis.

Statistical Analysis

Differential expression analysis for *HOTAIR* was performed on the Affymetrix HG U133 Plus 2.0 microarray gene expression data from 209 ependymal tumors. Statistical analysis and visualization of the data were performed using R “ggplot2” with the extension package “ggstatsplot” for statistical analysis (26). The data were nonparametric based on the Shapiro-Wilk test and visualization by density plots, therefore we used a nonparametric Kruskal-Wallis one-way analysis of variance (ANOVA) (29). A Bonferroni correction was used to correct for multiple comparisons.

For qPCR and ISH analysis, the Prism analysis software was used to perform the statistical analyses. Differences between 2 groups were compared using an unpaired *t*-test. Differences between 3 or more groups were analyzed using one-way ANOVA followed by Tukey’s post hoc test for multiple comparisons.

RESULTS

MPE Overexpress Posterior *HOX* Genes and LncRNA *HOTAIR*

We analyzed a dataset of 209 ependymal tumors across CNS compartments (Affymetrix Human Gene U133 Plus 2.0 microarray, GEO accession GSE66787) (Table; Supplementary Data Table S2). Hierarchical clustering was performed on *HOX* cluster gene expression and *HOTAIR* gene expression and sample data. All 8 MPE samples clustered together, and the spinal ependymomas clustered in a separate, adjacent group. MPEs were characterized by higher expression of posterior *HOX* genes, particularly the *HOXB*, *HOXC*, and *HOXD* clusters. MPEs overexpressed lncRNA *HOTAIR* compared with every other group (Fig. 1). Interestingly, the molecular subgroups of supratentorial and posterior fossa ependymomas were not fully segregated with hierarchical clustering on gene expressions. We further analyzed an additional spinal ependymoma dataset (Affymetrix Human Gene 1.1 ST Array, GEO accession GSE66787). This data set contains gene expression data for 20 MPE and 15 Grade II spinal ependymomas (Table; Supplementary Data Table S2). LncRNA *HOTAIR* expression data were unavailable in this dataset. MPE samples clustered together, with the exception of 3 samples with low baseline expression across the majority of *HOX* genes (Supplementary Data Fig. S1).

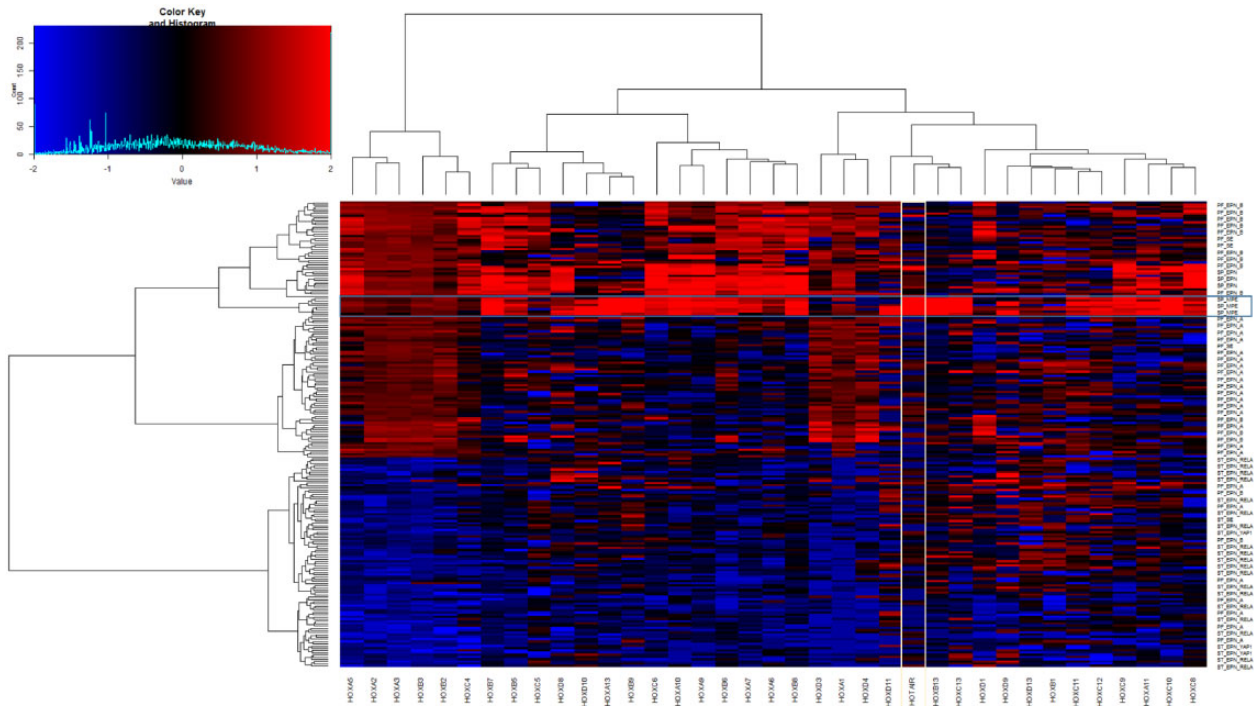


FIGURE 1. Gene expression heatmap from a dataset of 209 ependymal tumor samples. Rows represent HOTAIR and HOX gene expression and columns represent ependymoma samples. Overexpression is denoted by red and underexpression by blue. Gene expression was normalized to a mean of 0 and a standard deviation of 1 with z-scores >2 or <-2 were set to $2/-2$ to denote over and underexpression. The 8 MPE samples are encircled by the light blue box, and HOTAIR by the yellow box.

Grade II spinal ependymomas clustered separately with a distinct pattern of expression of *HOX* genes, corresponding to more anterior compartment *HOX* cluster genes.

The expression levels of selected genes were then compared among molecular subgroups of ependymomas, including MPE (n=8), spinal ependymoma (SP-EPN, n=11), spinal subependymoma (SP-SE, n=7), posterior fossa ependymoma group A (PF-EPN-A, n=72), posterior fossa ependymoma group B (PF-EPN-B, n=39), posterior fossa subependymoma (PF-SE, n=11), supratentorial ependymoma with YAP1 fusion (ST-EPN-YAP1, n=11), supratentorial ependymoma with RELA fusion (ST-EPN-RELA, n=49), and supratentorial subependymoma (ST-SE, n=8). On a gene-by-gene basis, MPEs significantly overexpressed *HOTAIR* compared with all other groups regardless of compartment ($p < 0.001$) (Fig. 2). MPE samples also showed higher expression of posterior *HOX* genes, such as *HOXA13*, *HOXB13*, and *HOXC13*. Interestingly, there was no differential expression of the *HOXD13* gene (Fig. 2). While *HOXD* cluster genes were overall expressed at low levels regardless of subgroup, *HOXD10* and *HOXD11* were highly expressed in MPE samples. There was no differential expression of *HOX* genes among the different molecular subgroups of the intracranial ependymomas.

It was previously reported that *HOTAIR* acts as in-trans regulator on the *HOXD* locus expression (30–32). We decided to further verify the lncRNA *HOTAIR* and expressions of 3

representative *HOXD* genes (*HOXD1*, 3 and 10), as “anterior” and “posterior” *HOX* genes, respectively, on our local ependymoma cohort. Since the different molecular subgroups of the IC-EPN were not fully delineated based on the basis of hierarchical clustering of *HOTAIR* and *HOX* gene expression, we decided to divide our cohort to 3 groups: MPE, SP-EPN, and IC-EPN. The clinical data including age at diagnosis, sex, histology diagnosis, and tumor grade are summarized in Table and detailed in Supplementary Data Table S2. Briefly, the mean age of diagnosis for MPE patients was 27 years (7–59 years). There is a male predominance, with a male-to-female ratio of 4:1. The mean age of diagnosis for IC-EPN was 27 years (1–62 years). The proportion of WHO grade I, II, III in IC-EPN is 19%, 48%, and 33%, respectively. Sixty-one percent of the IC-EPN were located in the posterior fossa and 39% was supratentorial placed. The male-to-female ratio for IC-EPN was 1.0:1.3. The demographic information was comparable to the 2 GEO cohorts (Table).

Frozen tissue of 8 MPE, 3 SP-EPN, and 20 IC-EPN were analyzed with real-time RT-PCR. In keeping with the bioinformatics analysis, *HOXD10* expression was significantly higher in MPE than SP-EPN and IC-EPN. The *HOXD1* and *HOXD3* gene expression did not show significant differences among the 3 groups (Fig. 3A). Notably, there was significant overexpression of *HOTAIR* in MPE. The lncRNA *HOTAIR* is nearly undetectable in SP-EPN and IC-EPN (Fig. 3B).

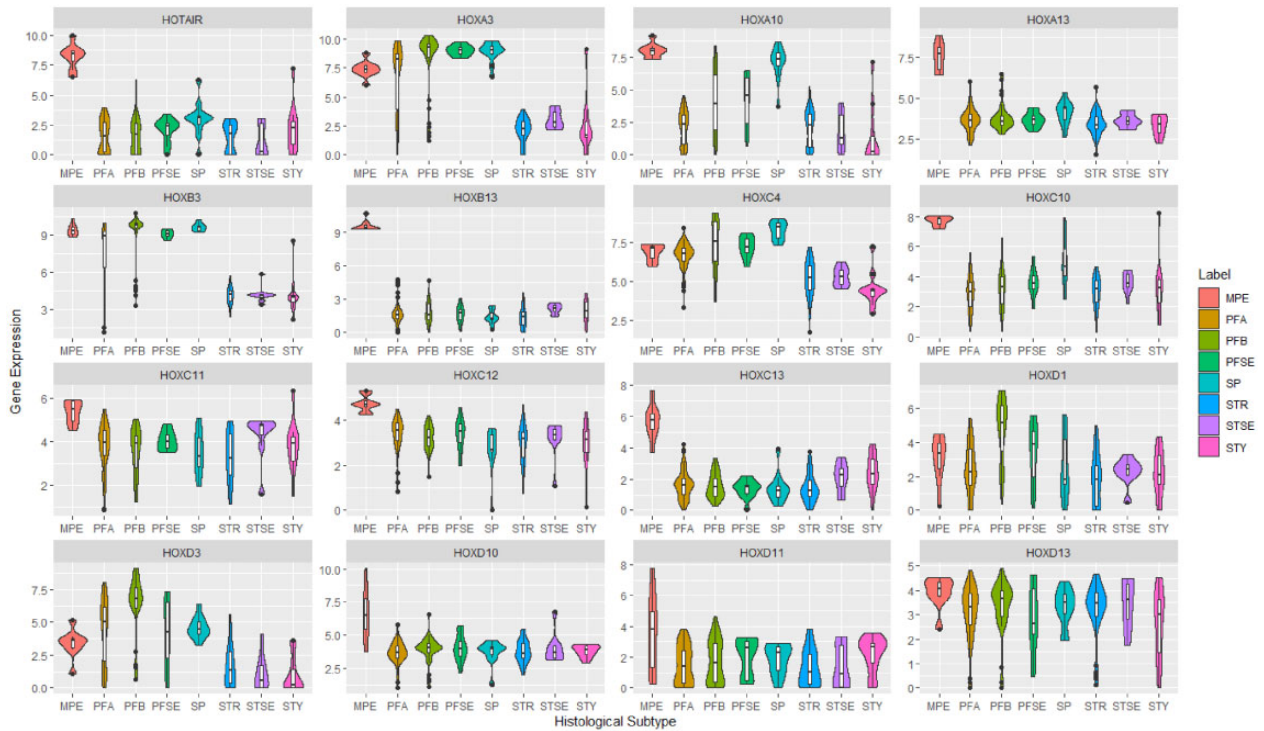


FIGURE 2. Violin plots with overlaid box plots of 16 selected genes. The center line of the box plot represents the median. The limits of the box plot represent the upper and lower quartiles. The whiskers represent the interquartile range and the dots represent outliers. The overlying violin represents the distribution of the sample values. The x-axis represents 9 molecular subtypes of EPNs—spinal myxopapillary ependymoma ([MPE], n=8), spinal ependymoma ([SP], n=11), posterior ependymoma type A ([PFA], n=72), posterior ependymoma type B ([PFB], n=39), posterior fossa subependymoma ([PFSE], n=11), supratentorial ependymoma with RELA fusion ([STR], n=49), supratentorial ependymoma with YAP1 fusion ([STY], n=11), supratentorial subependymoma ([STSE], n=8). The y-axis represents logarithmic RMA normalized gene expression with higher values indicating higher relative gene expression.

Overexpressed LncRNA HOTAIR Is Identifiable on Archived FFPE MPE Tissue

For routine clinical practice, frozen tumor tissue is not always available. We therefore decided to test the lncRNA HOTAIR expression in archived FFPE tissue. Nineteen FFPE ependymoma blocks were used to construct one TMA as described in the methods. Seven MPE, 6 SP-EPN, and 6 IC-EPN were included in this cohort. The typical histomorphology and immunoprofile of these tumors were well represented in most of the TMA cores (Fig. 4). MPEs were composed of glial cells with papillary architecture on a myxoid background. The tumor possessed GFAP-positive fibrillary process and abundant hyalinized vasculatures. Focally immunopositivity of pan cytokeratin (CK AE1/AE3) was also present on SP-MPE, but not on other ependymomas (Fig. 4).

RNA ISH was performed on the TMA, using a probe specific for human HOTAIR as described in the methods. A very robust HOTAIR expression was detected on a vast majority of the MPE TMA cores, but nearly undetectable in others (Fig. 5A–C). Quantification of the lncRNA HOTAIR ISH signal using QuPath revealed a 6-fold increase in MPE cores when compared with SP-EPN and IC-EPN (Fig. 5D).

The HOTAIR and HOXD10 Expression Is Not Elevated in Nonpendymal Spinal Tumors

Given the unique sacrolumbar location of MPE and the segmental patterning of HOX genes in the body A-P axis, we explored whether the overexpressed HOXD10 and lncRNA HOTAIR pertained to the caudal location or the unique tumorigenesis of MPE. Quantitative RT-PCR was further performed on 10 nonpendymoma spinal tumors (5 schwannoma, 3 neuroblastoma/ganglioneuroma, 1 pilocytic astrocytoma, and 1 osteochondroma) to analyze the expressions of HOTAIR and HOXD10. HOTAIR was nearly undetectable in all 10 nonpendymal spinal tumors, regardless of spinal segments. Except in one thoracic neuroblastoma, HOXD10 is expressed at a very low level in these spinal nonpendymoma tumors. Of note, one of the MPEs originated in the cervicothoracic segment, which also showed high expression levels of both HOTAIR and HOXD10, similar to the rest of the MPE group (Fig. 6).

DISCUSSION

MPE is a histologically and genetically distinct ependymoma subgroup, which almost exclusively arises from the terminal segment of the spinal cord (1, 33). Despite recent

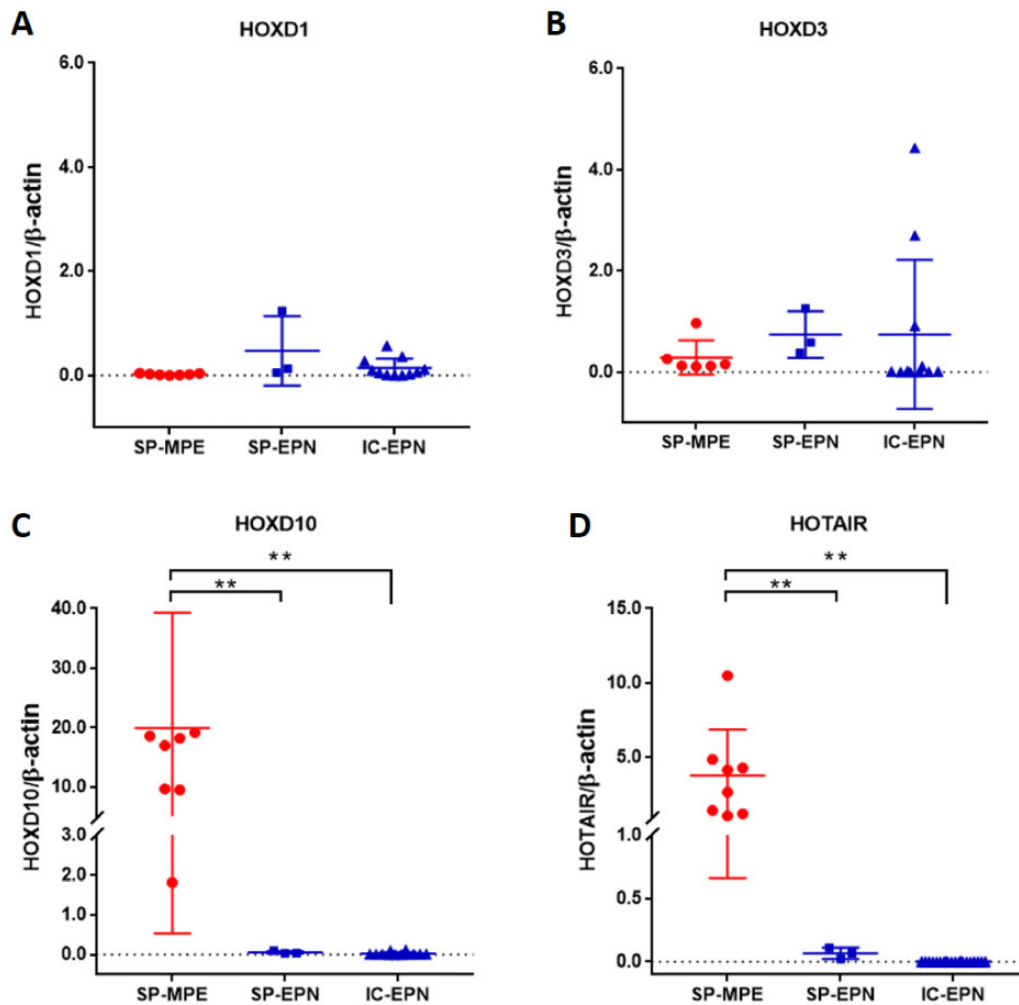


FIGURE 3. Quantitative RT-PCR analysis of *HOTAIR* and *HOXD* genes expression in ependymoma subgroups. The expression of *HOXD* 1 and 3 are low in all ependymoma groups (**A**, **B**). *HOXD*10 and lncRNA *HOTAIR* expression is upregulated in SP-MPE, in comparison to SP-EPN and IC-EPN (**C**, **D**). (SP-MPE, spinal myxopapillary ependymoma; SP-EPN, spinal ependymoma; IC-EPN, intracranial ependymomas; * $p < 0.05$; ** $p < 0.01$).

advances, little progress is made in the treatment of MPE. The current treatment of MPE is restricted to surgical resection and focal radiation for selected patients. The lack of targeted therapy is partly hindered by our poor understanding of the pathophysiology and tumorigenesis of this rare tumor type. The present study incorporated bioinformatics analysis, quantitative RT-PCR, and RNA ISH to identify a distinct expression profile of *HOX* genes and the lncRNA *HOTAIR* in MPE.

A study by Barton et al reported overexpression of a handful of *HOX* genes in 5 pediatric MPE cases, compared with IC-EPNs. We confirmed this observation and expanded the findings to include adult patients. The average age was 27 years in our MPE cohort and 31 years in the 2 GEO databases. Elevated posterior *HOX* genes were observed in MPEs of all age groups.

The roles of *HOX* genes in tumorigenesis are complex and are reviewed by Shah and Sukumar in their excellent opinion article (9). Particular *HOX* genes can play tumor repressive

or oncogenic effects in different organ and tumor types. Aberrant *HOX* gene expression with temporospatial deregulation is usually associated with certain tumors. For instance, esophageal carcinomas express higher levels of 5' *HOX* genes, which are normally not seen in a foregut structure. Interestingly, the spatial arrangement of *HOX* genes was relatively preserved in the ependymomas, with higher posterior *HOX* gene expression in MPE, consistent with their spatial collinearity during development. Similar arrangements were also observed in clival and sacral chordomas: Expression of the 5' *HOXA*10 is significantly higher in sacral chordomas in comparison to the clivus counterpart (30). This differential expression may suggest an oncofetal gene regulatory mechanism specific to tumor anatomical location. However, the overexpression of *HOXD*10 and *HOTAIR* were not observed in non-MPE spinal tumors at the same spinal segment, suggestive of an MPE-specific upregulation. *HOXD*4 was among the most common super-enhancers identified in the PF-EPN-B molecular subgroup by

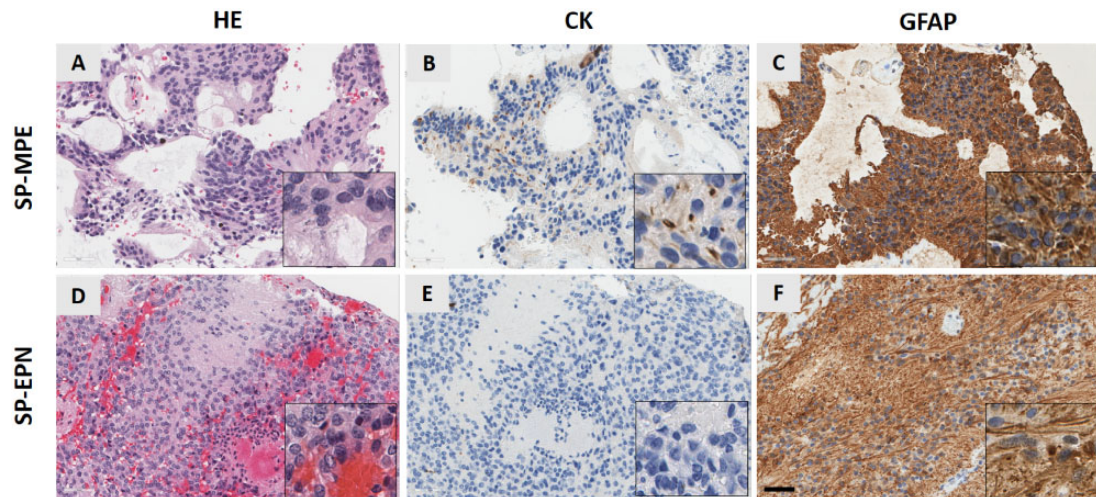


FIGURE 4. Histomorphology and immunoprofile are well retained in most of the TMA cores. SP-MPEs are composed of glial cells with papillary architecture on a myxoid background (A). The tumor cells are focally positive for CK AE1/AE3 (B) and diffusely positive for GFAP (C). SP-EPN contains fibrillary background (D), but is immunonegative for CK (E) and positive for GFAP (F). (HE, hematoxylin eosin; CK, cytokeratin; GFAP, glial fibrillary acidic protein; SP-MPE, spinal myxopapillary ependymoma; SP-EPN, spinal ependymoma. Scale bar: 50 μ m).

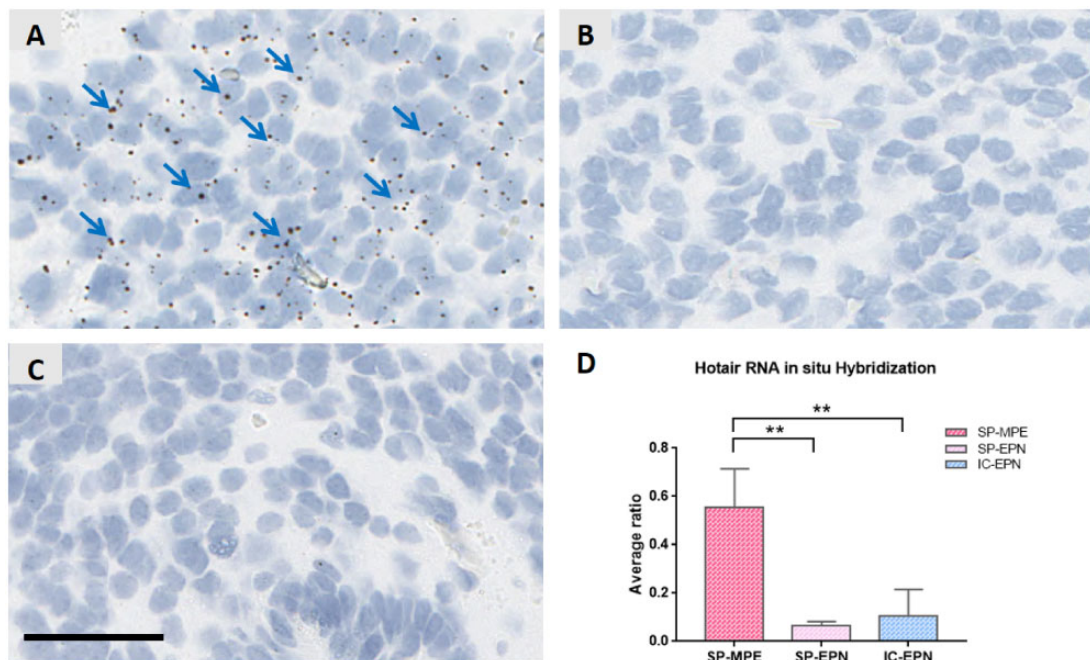


FIGURE 5. RNA in situ hybridization of HOTAIR on the ependymoma tissue microarray. RNA ISH revealed a robust HOTAIR expression in SP-MPE (A), but not in SP-EPN (B) or IC-EPN (C). There is a nearly 6-fold increase of HOTAIR expression in SP-MPE, when compared with SP-EPN and IC-EPN (D). (SP-MPE, spinal myxopapillary ependymoma; SP-EPN, spinal ependymoma; IC-EPN, intracranial ependymomas; Arrows in A: positive signal of RNA ISH with probes to human HOTAIR. Scale bar: 50 μ m; * $p < 0.05$; ** $p < 0.01$).

oncogenic enhancer profiling (3). Spinal ependymoma and MPE were not reported in that study.

The controversy over the effects of lncRNA HOTAIR regulating HOXD genes added another layer of complexity to these findings. The coexpression of high levels of HOTAIR and HOXD10 in the MPE were unexpected. A well-accepted

function of HOTAIR is that during development, HOTAIR acts as a trans-acting repressor of HOXD genes by recruiting PRC2, in turn methylating histone H3 and silencing the HOXD cluster expression (32). More specifically, in Hotaair conditional knockout (KO) mice, the KO of Hotaair led to a loss of H3K27me3 and a gain of H3K4me3 at HoxD

2012 and 2014, and yet the hybridization signal of *HOTAIR* is surprisingly well retained. Recently, circulating lncRNAs have also been shown to be stable in serum and detectable in peripheral blood. In particular, serum *HOTAIR* is being tested for its diagnostic and prognostic value in glioblastoma (40).

Personalized medicine with targeted oncology therapy is usually determined by identifying driver mutations of the primary tumor. Ependymomas, however, are one exception. Ependymomas harbor no recurrent somatic mutations and appear to be mostly epigenetically driven (2, 39, 40, 41). The C11orf95-*RELA* fusion defines a supratentorial ependymoma with poor prognosis (ST-EPN-*RELA*) (4). Based on the CpG island methylation phenotype (CIMP), the posterior fossa ependymomas are subdivided into 2 molecular groups: PF-EPN-A and PF-EPN-B. The PF-EPN-A exhibits CIMP-positive phenotype (CpG island hypermethylation) and bears a more aggressive clinical behavior and requires intensive therapy (42). However, little is known on MPE. Studying the 2 GEO data sets and our local cohort allowed us to incorporate gene expression data from a relatively large number of cases for this rare tumor type. We are reporting for the first time an epigenetic signature of MPE, where the lncRNA *HOTAIR* is specifically upregulated in MPEs, but not in other ependymoma subgroups or spinal nonependymoma tumors. Apart from its diagnostic value, targeting *HOTAIR* may serve as a promising therapeutic strategy since this lncRNA is augmented in MPE. Modulation of lncRNA expression by siRNAs or other nucleic acid-based therapies have been shown to improve the treatment efficacy in many different cancers (31).

We conclude by acknowledging the limitation of this study. Due to the scarcity of reliable MPE tumor cell line and difficulty to obtain patient-derived primary MPE culture, the function of *HOTAIR* in MPE and its roles in regulating the expression of *HOXD* genes remain unexplained in this tumor. Future studies are needed to explore the mechanisms underlying *HOTAIR*-mediated regulation of *HOX* genes during MPE tumorigenesis.

ACKNOWLEDGMENT

We thank Dr Lee Cyn Ang and Dr Yuanyuan Gu for reviewing this manuscript and providing comments.

REFERENCES

- Louis DN, Ohgaki H, Wiestler OD, et al. *WHO Classification of Tumours of the Central Nervous System*. Lyon, France: IARC Press 2016:106–14.
- Ellison DW, Aldape KD, Capper D, et al. cIMPACT-NOW update 7: Advancing the molecular classification of ependymal tumors. *Brain Pathol* 2020; 0: 1–4. doi:10.1111/bpa.12866 [Epub ahead of print]
- Mack SC, Pajtlar KW, Chavez L, et al. Therapeutic targeting of ependymoma as informed by oncogenic enhancer profiling. *Nature* 2018;553: 101–5
- Pajtlar KW, Witt H, Sill M, et al. Molecular classification of ependymal tumors across all CNS compartments, histopathological grades, and age groups. *Cancer Cell* 2015;27:728–43
- Barton VN, Donson AM, Kleinschmidt-Demasters BK, et al. Unique molecular characteristics of pediatric myxopapillary ependymoma. *Brain Pathol* 2010;20:560–70
- Gu S, Gu W, Shou J, et al. The molecular feature of *HOX* gene family in the intramedullary spinal tumors. *Spine* 2017;42:291–7
- McGinnis W, Krumlauf R. Homeobox genes and axial patterning. *Cell* 1992;68:283–302
- Shah N, Sukumar S. The *Hox* genes and their roles in oncogenesis. *Nat Rev Cancer* 2010;10:361–71
- Selleri L, Bartolomei MS, Bickmore WA, et al. A *Hox*-embedded long noncoding RNA: Is it all hot air? *PLoS Genet* 2016;12:e1006485
- Dasen JS. Long noncoding RNAs in development: Solidifying the Lncs to *Hox* gene regulation. *Cell Rep* 2013;5:1–2
- Philippidou P, Dasen JS. *Hox* genes: Choreographers in neural development, architects of circuit organization. *Neuron* 2013;80:12–34
- Tang Q, Hann SS. *HOTAIR*: An oncogenic long non-coding RNA in human cancer. *Cell Physiol Biochem* 2018;47:893–913
- Xu S, Kong D, Chen Q, et al. Oncogenic long noncoding RNA landscape in breast cancer. *Mol Cancer* 2017;16:129
- Li L, Wang Y, Song G, et al. *HOX* cluster-embedded antisense long noncoding RNAs in lung cancer. *Cancer Lett* 2019;450:14–21
- He Y, Meng X-M, Huang C, et al. Long noncoding RNAs: Novel insights into hepatocellular carcinoma. *Cancer Lett* 2014;344:20–7
- Li T, Mo X, Fu L, et al. Molecular mechanisms of long noncoding RNAs on gastric cancer. *Oncotarget* 2016;7:8601–12
- Tatangelo F, Di Mauro A, Scognamiglio G, et al. Posterior *HOX* genes and *HOTAIR* expression in the proximal and distal colon cancer pathogenesis. *J Transl Med* 2018;16:350
- Li Q, Dong C, Cui J, et al. Over-expressed lncRNA *HOTAIRM1* promotes tumor growth and invasion through up-regulating *HOXA1* and sequestering *G9a/EZH2/Dnmts* away from the *HOXA1* gene in glioblastoma multiforme. *J Exp Clin Cancer Res* 2018;37:265
- Vladoiu MC, El-Hamamy I, Donovan LK, et al. Childhood cerebellar tumours mirror conserved fetal transcriptional programs. *Nature* 2019; 572:67–73
- Holland PWH, Booth HAF, Bruford EA. Classification and nomenclature of all human homeobox genes. *BMC Biol* 2007;5:47
- Mack SC, Agnihotri S, Bertrand KC, et al. Spinal myxopapillary ependymomas demonstrate a Warburg phenotype. *Clin Cancer Res* 2015;21: 3750–8
- Durink S, Spellman PT, Birney E, et al. Mapping identifiers for the integration of genomic datasets with the R/Bioconductor package *biomaRt*. *Nat Protoc* 2009;4:1184–91
- Durink S, Moreau Y, Kasprzyk A, et al. BioMart and Bioconductor: A powerful link between biological databases and microarray data analysis. *Bioinformatics* 2005;21:3439–40
- Team RC. R: A language and environment for statistical computing, 2013. Available from: <http://www.r-project.org/>. (last accessed on August 24, 2020)
- Wickham H. *ggplot2: Elegant Graphics for Data Analysis*, 2016. New York: Springer-Verlag. Available from: <https://ggplot2.tidyverse.org>. (last accessed on August 24, 2020)
- Patil I. *ggstatsplot: “ggplot2” Based Plots with Statistical Details*, 2018. Available from: <https://cran.r-project.org/package=ggstatsplot>. (last accessed on August 24, 2020)
- Bankhead P, Loughrey MB, Fernández JA, et al. QuPath: Open source software for digital pathology image analysis. *Sci Rep* 2017;7:1–7
- Loughrey MB, Bankhead P, Coleman HG, et al. Validation of the systematic scoring of immunohistochemically stained tumour tissue microarrays using QuPath digital image analysis. *Histopathology* 2018;73: 327–12
- Kruskal WH, Wallis WA. Use of ranks in one-criterion variance analysis. *J Am Stat Assoc* 1952;47:583–621
- Jäger D, Barth TFE, Brüderlein S, et al. *HOXA7*, *HOXA9*, and *HOXA10* are differentially expressed in clival and sacral chordomas. *Sci Rep* 2017;7:2032
- Bhan A, Soleimani M, Mandal SS. Long noncoding RNA and cancer: A new paradigm. Vol. 77, *Cancer Research*. American Association for Cancer Research, Inc. 2017:3965–81
- Rinn JL, Kertesz M, Wang JK, et al. Functional demarcation of active and silent chromatin domains in human *HOX* loci by noncoding RNAs. *Cell* 2007;129:1311–23
- Connolly ID, Ali R, Li Y, et al. Genetic and molecular distinctions in spinal ependymomas: A review. *Clin Neurol Neurosurg* 2015;139:210–5
- Schorderet P, Duboule D. Structural and functional differences in the long non-coding RNA *Hota* in mouse and human. *PLoS Genet* 2011;7: e1002071
- Lee JC, Sharifai N, Dahiya S, et al. Clinicopathologic features of anaplastic myxopapillary ependymomas. *Brain Pathol* 2019;29:75–84

36. Estrozi B, Queiroga E, Bacchi CE, et al. Myxopapillary ependymoma of the posterior mediastinum. *Ann Diagn Pathol* 2006;10:283–7
37. McEachron KR, Gaertner WB. Extradural sacrococcygeal subcutaneous ependymoma misdiagnosed as pilonidal disease: Case report and review of the literature. *J Surg Case Rep* 2016;7: 1–3.
38. Shelekhova KV, Egorenkov VV, Kheinstein VA, et al. Myxopapillary ependymoma of lumbar soft tissue: A case report with gene expression evaluation. *Int J Surg Pathol* 2018;26:364–9
39. Ye W-B, Zhou J-P, Xu Y-Q, et al. Primary mediastinal ependymoma: A case report and literature review. *Medicine (Baltimore)* 2019;98:e17686
40. Tan SK, Pastori C, Penas C, et al. Serum long noncoding RNA HOTAIR as a novel diagnostic and prognostic biomarker in glioblastoma multiforme. *Mol Cancer* 2018;17:74
41. Feinberg AP. The key role of epigenetics in human disease prevention and mitigation. *N Engl J Med* 2018;378:1323–34
42. MacK SC, Witt H, Piro RM, et al. Epigenomic alterations define lethal CIMP-positive ependymomas of infancy. *Nature* 2014;506:445–50